the speed of time to increase—there is a clinical reason for this nature-related, aging phenomenon. We then showed that nurture-related or experiential factors could also affect our perceived speed of time. Indeed, although the results should be considered preliminary, our analysis suggests that nurture and nature may have a comparable impact on our perceived speed of time. When controlled for nature (i.e., age), the nurture-related experiential data suggest that we perceive time to be moving faster over time, due to accelerating "future shocks."

Clearly, our current effort is at best exploratory. Further surveys and analyses should be undertaken to validate and extend our findings. Issues to be considered include: What would be the results of a survey where subjects were asked to estimate a 2-min or even a 5-min interval? How would the results differ in different locales or countries? (Our survey data was gathered from a limited group; to further generalize our findings, it would be necessary to recreate the survey with a larger sample, randomized over both geographic and demography.) How does nurture and nature interrelate in regard to our perception of time and speed of time? How do group activities affect this perception? What is the impact of Internet time on this perception?

Finally, it should be noted that understanding the way we perceive the speed of time over time is not only an important endeavor in its own right, but it also has potentially significant impact on our ability to cope, on our work productivity, on our lifestyle, indeed on all aspects of our life. Levine [10], for example, cites a study of Peace Corps volunteers that concluded that one of the three greatest adjustment difficulties was "general pace of life," exceeded only by "language spoken."

REFERENCES

[1] F. Macar, V. Pouthas, and W. J. Friedman, Eds., *Time, Action, and Cognition*. Boston, MA: Kluwer, 1992.

[2] T. Rammsayer, "Effect of body core temperature and brain dopamines on timing processes in humans," *Biologic. Psychol.*, vol. 46, no. 2, pp. 169–192, Aug. 1997.

[3] A. Angrilli, P. Cherubini, A. Pavese, and S. Manfredini, "The influence of affective factors on time perception," *Perception Psychophys.*, vol. 59, no. 6, pp. 972–982, Aug. 1997.

[4] C. Lustig and W. Meck, "Paying attention to time as one gets older," *Psychologic. Sci.*, vol. 12, no. 6, pp. 478–484, Nov. 2001.

[5] C. W. Bradberry, "Acute and chronic dopamine dynamics in a nonhuman primate model of recreational cocaine use," *J. Neurosci.*, vol. 20, no. 18, pp. 7109–15, Sep. 2000.

[6] H. J. Shaffer and S. E. Hyman, "Drugs and the brain," *Harvard Mahoney Neurosci. Inst. Lett.*, vol. 2, Sep. 1993.

[7] A. Toffler, *Future Shock*. New York: Random House, 1970.

[8] J. Gleick, *Faster*. New York: Vintage, 1999.

[9] T. J. Cottle, *Perceiving Time*. New York: Wiley, 1976.

[10] L. P. Lipsitt, "Time passeth," *Brown Univ. Child Adolescent Lett.*, vol. 16, no. 1, p. 8, Jan. 2000.

[11] R. V. Levine, "The pace of life," *Amer. Scientist*, vol. 78, no. 5, pp. 450–459, Sept.–Oct. 1990.

[12] S. Blakeslee, "Running late? Researchers blame your aging brain," *New York Times*, p. 37, Mar. 1998.

[13] M. G. Flaherty and M. D. Meer, "How time flies: Age, memory, and temporal compression," *Sociologic. Quart.*, vol. 35, no. 4, pp. 705–21, Nov. 1994.

[14] *Transportation Indicators for Motor Vehicles and Airlines*: U. S. Census Bureau, 1999.

[15] "Issue Years and Patent Numbers,", 2000.

[16] *Multifactor Productivity Trends*: U. S. Bur. Labor Statist., 1997.

Bio-Mimetic Trajectory Generation Based on Human Arm Movements With a Nonholonomic Constraint

Toshio Tsuji, Yoshiyuki Tanaka, and Makoto Kaneko

***Abstract*—In this paper, a bio-mimetic trajectory of robots for manipulating a nonholonomic car is generated with a time base generator (TBG). In order to reveal what kind of trajectories the robots should generate for the given task, experiments with human subjects were performed. It has been shown that a human generates the trajectory with a single- or double-peaked velocity profile according to the geometrical conditions of the car. Then, bio-mimetic trajectories were generated by modeling the observed primitive profiles with the TBG and also compared with the human trajectories.**

***Index Terms*—Human movements, nonholonomic constraints, time base generator (TBG), trajectory generation.**

I. INTRODUCTION

Remarkable developments of human-shaped robots have been achieved in recent years [1], [2]. However, no matter how similar, from a cosmetic point of view, to a human the robot is, it may not be accepted to cowork or coexist with human beings in daily activities if the robot cannot move or perform a given task with human-like movements. In this paper, human arm movements are examined and modeled in order to design human-like movements for robots.

There have been many studies on the mechanism of human arm movements [3]–[7]. For example, Morasso [3] examined reaching movements of a two-joint arm restricted to a horizontal plane and found the common invariant kinematic features that a human usually moves his hand along a roughly straight path with a bell-shaped velocity profile. As an explanation for the control mechanism of such human movements, many models have been proposed: "a minimum jerk model" [4], "a minimum torque-change model" [5], and "a VITE model" [6]. The first and second models assert that the underlying mechanism is feed-forward control, while the last one is considered as feedback control. All of these models can generate hand trajectories in good agreement with experimental data.

Also, Morasso *et al.* [7] proposed a time base generator (TBG) which generates a time-series with a bell-shaped velocity profile and showed that a straight/curved hand trajectory can be generated by synchronizing a translational/rotational velocity of the hand with the TBG signal. Then, Tsuji *et al.* [8], [9] applied the TBG to the motion control of a nonholonomic robot and a redundant manipulator. Moreover, Tanaka *et al.* [10] developed a trajectory generation method based on the artificial potential field approach combining a time scale transformation and the TBG. These studies, however, did not handle the trajectory generation with any constraints, although human movements in daily activities are often constrained by the task environments.

Generally, geometrical constraints can be classified into two types: holonomic constraints and nonholonomic constraints. Some studies have been reported on human arm movements with holonomic constraints, such as the hand force patterns in the crank rotation tasks

Manuscript received June 6, 2000; revised September 20, 2002. This work was supported in part by the Scientific Research Foundation of the Ministry of Education, Science, Sports and Culture, Japan (11555113 and 11650450). This paper was recommended by Associate Editor W. A. Gruver.

The authors are with the Graduate School of Engineering, Hiroshima University, Higashi-Hiroshima 739-8527, Japan (e-mail: tsuji@bsys.hiroshima-u.ac.jp).

Digital Object Identifier 10.1109/TSMCA.2002.807031

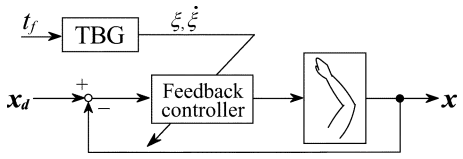

Fig. 1. Block diagram of the TBG model for human hand reaching movements.

[11], [12], the dynamic characteristics of hand motion in the manual tracking control tasks with a linear table [13]. However, as far as we know, there is no study on human movements with nonholonomic constraints.

This paper aims to reproduce a human hand trajectory in a nonholonomic-constrained task [14]. Manipulation of a nonholonomic toy car from one point to another was chosen as the target task. First, experiments with human subjects were conducted in order to reveal what kind of hand trajectories a human would generate in this task. Through the observation of human movements, it was found that a human generates three types of primitive spatial trajectories: a straight trajectory, an S-shaped trajectory, and a quadrantal-arc trajectory. Also, depending on the experimental conditions of the car, a switching point appears in generating trajectories. In addition, a hand velocity profile in the primitive spatial patterns can be classified into two types: a single-peaked profile and a double-peaked profile. By modeling these velocity profiles with the TBG, a human-like trajectory of robots performing the same task was generated.

This paper is organized as follows: Section II proposes a new TBG model and describes a TBG-based trajectory generation method for robots. In Section III, the characteristics of a human trajectory in the nonholonomic constrained task is found through experiments with human subjects. Then, a feedback controller to generate human-like trajectories is designed by means of the TBG-based method in Section IV. Finally, the simulation results are shown and compared with the human trajectory in Section V.

II. Trajectory Generation Based on the TBG

A. TBG Model

The control model of human hand trajectory generation using a TBG [8], [9] is represented by the block diagram of Fig. 1. The TBG, $\xi(t)$, is a nonincreasing scalar function and generates a bell-shaped velocity profile satisfying $\xi(0) = 1$ and $\xi(t_f) = 0$ with the convergence time t_f.

The feedback controller in Fig. 1 outputs a command in such a way that an error between a current position x and a target position x_d is forced to synchronize with the TBG signal so that a human hand can reach the target with a bell-shaped velocity profile at the specified time t_f. However, human arm movements when performing ordinary work during daily activities are often affected by the task environments, so that the velocity profile often has some asymmetric distortion. Therefore, in this paper, a TBG considering the generation of asymmetric profiles [14] is proposed. The dynamics of ξ are defined as follows:

$$\dot{\xi} = -\gamma \xi^{\beta_1}(1-\xi)^{\beta_2} \tag{1}$$

where the parameters γ and β_i $(i = 1, 2)$ are positive constants under $0 < \beta_i < 1$. The velocity profile of the TBG can be adjusted by changing β_i, while the convergence time t_f is calculated with the parameter γ and the gamma function $\Gamma(\bullet)$ as

$$t_f = \int_0^{t_f} dt = \frac{\Gamma(1-\beta_1)\Gamma(1-\beta_2)}{\gamma\Gamma(2-(\beta_1+\beta_2))}. \tag{2}$$

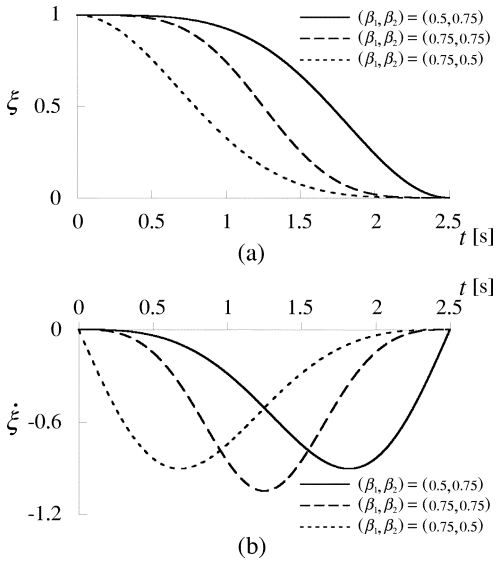

Fig. 2. Change of the dynamic behavior of the TBG depending on β_i with the convergence time $t_f = 2.5$ [s] (a) Time courses of ξ. (b) Velocity profiles of ξ.

Thus, the system converges to the equilibrium point $\xi = 0$ in the finite time t_f if γ in (1) is chosen as

$$\gamma = \frac{\Gamma(1-\beta_1)\Gamma(1-\beta_2)}{t_f\Gamma(2-(\beta_1+\beta_2))}. \tag{3}$$

Fig. 2 shows the time histories of ξ and $\dot{\xi}$ using the parameters $(\beta_1, \beta_2) = (0.75, 0.5)$, (0.75, 0.75) and (0.5, 0.75) with the convergence time $t_f = 2.5$ [s]. It can be seen that a velocity profile of the TBG signal can be regulated by changing β_i so that the asymmetric profile as well as the symmetric profile can be generated.

B. Time-Scaled Artificial Potential Field

Tanaka *et al.* [10] have developed a trajectory generation method for robots by means of the time scale transformation with the TBG in the framework of the artificial potential field approach (APFA), which can generate a human-like trajectory. The block diagram of the controlled robot in this method can be expressed by exchanging the pictorial shape of human arm in Fig. 1 with that of a robotic arm. This subsection describes the TBG-based method through deriving a feedback controller of robots.

Generally, the kinematics of nonredundant robots can be described as

$$\dot{\boldsymbol{x}} = \boldsymbol{G}(\boldsymbol{x})\boldsymbol{U} \tag{4}$$

where $\boldsymbol{x}, \boldsymbol{U} \in \Re^n$ are the position and the input vectors of the robots, respectively, and it is assumed that $\det \boldsymbol{G}(\boldsymbol{x}) \neq 0$.

Then, the relationship between actual time t and virtual time s is defined using the TBG signal $\xi(t)$ with a positive constant p as

$$a(t) = \frac{ds}{dt} = -p\frac{\dot{\xi}}{\xi} \tag{5}$$

where a continuous function $a(t)$ is called the time scale function [16]. From (1) and (5), virtual time s can be derived as follows:

$$s = \int_0^t a(t)dt = -p\ln\xi(t). \tag{6}$$

It is obvious that virtual time s in (6) can be controlled by ξ and never goes backward against actual time t. Thus, the system given in (4) can be rewritten in virtual time s defined by (6) as follows:

$$\frac{d\boldsymbol{x}}{ds} = \frac{d\boldsymbol{x}}{dt}\frac{dt}{ds} = \boldsymbol{G}(\boldsymbol{x})\boldsymbol{U}_s \tag{7}$$

where

$$\boldsymbol{U}_s = \frac{1}{a(t)}\boldsymbol{U}. \tag{8}$$

On the other hand, the APFA [8], [9] sets a potential function $V(\boldsymbol{x})$ which is minimized at a goal position $\boldsymbol{x}_d$ set in the task space. By applying a virtual attractive force to the goal position, the robot can reach the target in infinite time. An example of such a feedback controller $\boldsymbol{U}_s$ is given as

$$\boldsymbol{U}_s = -\boldsymbol{G}^{-1}(\boldsymbol{x})\left(\frac{\partial V}{\partial \boldsymbol{x}}\right)^T. \tag{9}$$

By using inverse time-scaling from virtual time s to actual time t for the feedback controller $\boldsymbol{U}_s$ designed by the APFA in virtual time s, a feedback control law $\boldsymbol{U}$ in actual time t is derived as

$$\boldsymbol{U} = -a(t)\boldsymbol{G}^{-1}(\boldsymbol{x})\left(\frac{\partial V}{\partial \boldsymbol{x}}\right)^T. \tag{10}$$

By using the derived controller $\boldsymbol{U}$, the system (4) in the actual time scale converges the equilibrium point at the specified time t_f. That is, it is able to generate a spatio-temporal trajectory from the initial to the target position with the specified convergent time t_f.

The method has been applied to produce a human-like trajectory for robots [10], but any constraints have not been considered in generating trajectories. To the contrary, this paper focus on the trajectory generation with nonholonomic constraints for robots by using the TBG-based method.

III. Human Arm Movements With a Nonholonomic Constraint

As an example of nonholonomic constrained tasks, manipulation of a nonholonomic car from one point to another was chosen. First, the trajectory generation experiments with human subjects were performed so as to show what kind of trajectories a human would generate for the task. Then, general characteristics of the observed human strategies for the target task were found for the human-like trajectory generation of robots.

A. Experimental Conditions

Fig. 3 shows the experimental apparatus. A subject is instructed to sit on his heels and move the nonholonomic model car, which has two wheels and one spherical wheel as shown in Fig. 3(b), from an initial to a target point [see Fig. 3(a)]. In the experiment, the translational velocity v and the angular velocity ω of the car are calculated as human hand velocities by measuring movements of the car and subject's arm with a stereo camera system (Quick MAG, Ouyou Keisoku Kenkyusyo, Inc.).

The employed camera system can detect a three-dimensional (3–D) position of a color marker [marked with ◯ in Fig. 3(b)] attached at a measurement point (maximum of eight points) from a couple of two-dimensional (2-D) image sequences taken by two CCD cameras in real time. Both v and ω were calculated through the digital differentiation of the marker's smoothed positional data, where the cut-off frequency

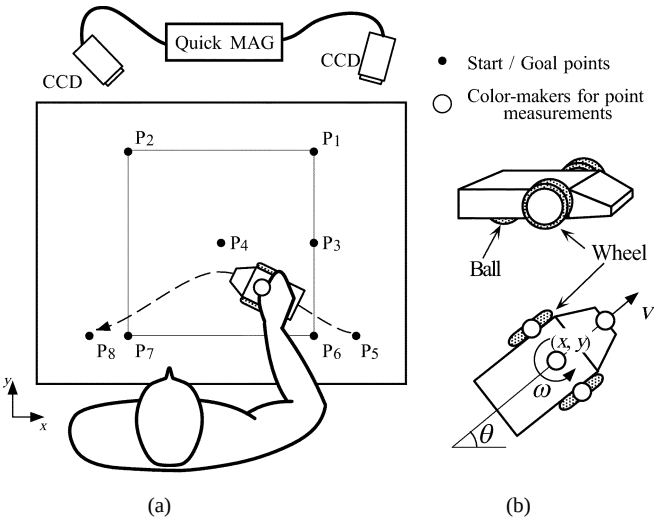

Fig. 3. Experimental apparatus. (a) Schematic overview of experiments. (b) Nonholonomic car.

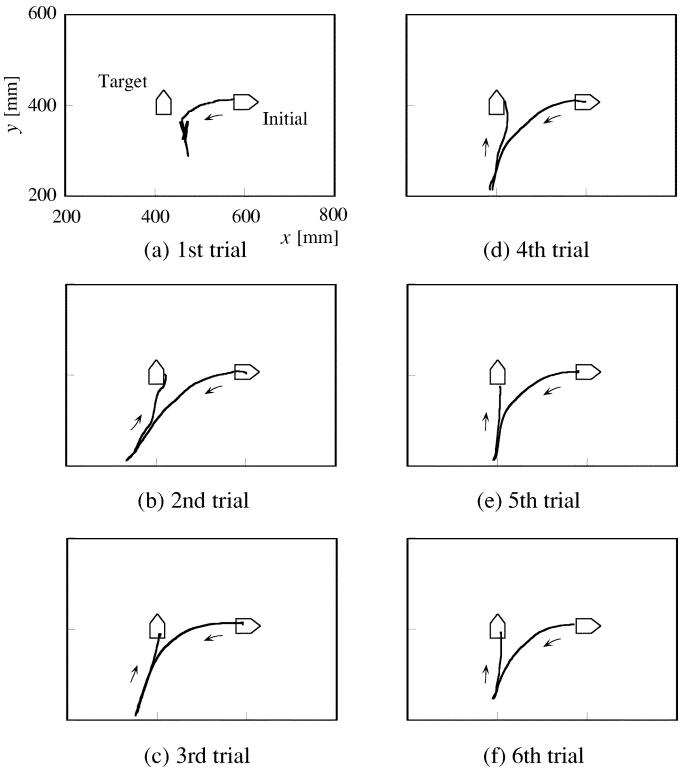

Fig. 4. Learning process of the trajectory generation with a nonholonomic constraint.

of the second-order Butterworth filter is automatically determined with Winter's method [15].

With this apparatus, a series of experiments was carried out with nine subjects (male university students), where the order of experimental conditions and the number of trials were changed for each subject.

B. Observation of Primitive Trajectories

All subjects generated complicated trajectories or could not move the car to the specified target point in the first several trials, but could generate stable spatial trajectories soon. Fig. 4 shows an example of the skill acquisition process on the target task with the initial point P_3 and the target point P_4. The initial and target postures of the car were set

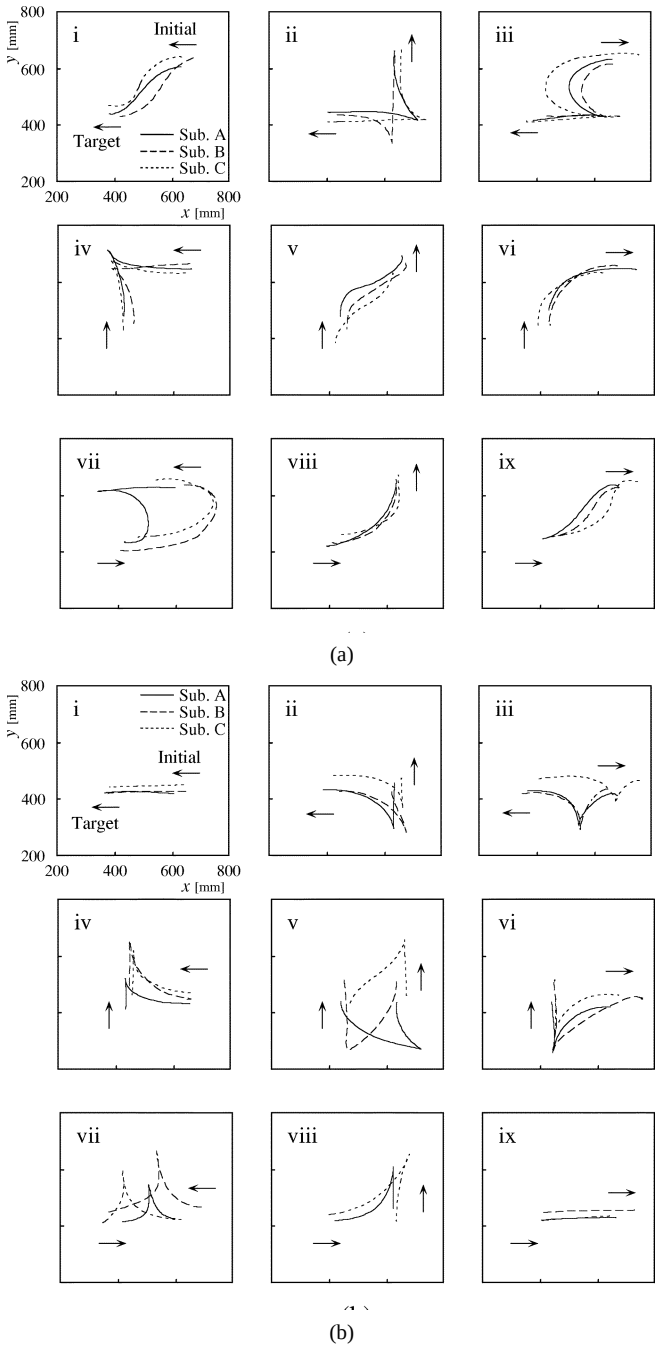

Fig. 5. Maps of generated trajectories with the different experimental conditions. (a) Initial point is set at P_1. (b) Initial point is set at P_3.

as 0, $\pi/2$ [rad], respectively. As shown in Fig. 4, the subject could not move the car to the goal point in the first trial [Fig. 4(a)], but after that generated almost the same spatial trajectory.

Fig. 5 shows a representative example of the spatial trajectories by the practiced subjects with the different initial and target conditions of the car. In the figure, an arrow shows the initial/target direction of the car; and the trajectories by each subject are distinguished by the type of line. Also, the initial points in Fig. 5(a) and (b) are set at P_1 and P_3, respectively, with the target point P_4 under $\theta_0 = \theta_d = 0$ [rad].

It can be seen from Fig. 5 that the subjects generate different trajectories according to the specified initial and target conditions, and that most of them select the same motion patterns although some individual differences are observed in the trajectories such as Fig. 5(a)-vii, (b)-v and (b)-vii. The generated spatial patterns have been classified into three groups in this paper: a straight trajectory; a curved trajectory; and a switching trajectory. From kinematical features of the observed switching trajectories, it can be suggested that a switching trajectory is produced by connecting a straight line with a quadrantal-arc trajectory. Furthermore, although the subjects can generate a variety of curved trajectories voluntarily, two types of the curved trajectories have been mainly observed under the specified conditions: the S-shaped trajectory as shown in Fig. 5(a)-i, v, ix; and the quadrantal-arc trajectory as shown in Fig. 5(a)-vi, viii.

From the experimental results, it was found that a straight trajectory, an S-shaped trajectory and a quadrantal-arc trajectory can be considered as the primitive spatial strategies of a human in manipulating a nonholonomic car. To investigate the velocity profile of these primitive patterns, the following additional experiments were carried out.

1) To move the model car from the initial point P_5 to the target point P_8 under the postural condition $\theta_0 = \theta_d = \pi$ [rad]: a subject is asked to generate a vertically curved spatial trajectory like the dotted line shown in Fig. 3(a) as the trials goes on. This experiment is planned to investigate a relation between the curvature of spatial trajectories and velocity profiles.
2) To move the model car from the initial point P_6 to the target point P_2 under the postural condition $\theta_0 = \theta_d = \pi/2, \pi$ [rad].
3) To move the model car from the initial points P_1, P_2, P_6, P_7 to the target point P_4 under $\theta_0 = \pi/2$ [rad] and $\theta_d = \pi$ [rad]. The initial points are located at the vertices of a square whose sides are 400 mm long and the target point is positioned at the center of the square.

Fig. 6 shows a typical example of the observed spatial trajectories and translational velocity profiles of the car, where the translational velocity v is normalized by its maximum value $v_{\max}$ and the time t by a measured movement time t_f from the initial to the target point for each trial. The trajectories in each figure [Fig. 6(a)–(c)] were generated by the different practiced subjects.

It can be seen from Fig. 6(a) that the straight trajectories have a single-peaked velocity profile which peaks around $t = (t_f/2)$ and that the velocity profile tends to be more sharply double-peaked as the curvature increases. As similar as the out-curved trajectory under the experimental condition 1, the S-shaped trajectories in Fig. 6(b) have a double-peaked velocity profile.

On the other hand, under the condition 3), the subjects generated two kinds of spatial trajectories according to the specified initial point as shown in Fig. 6(c): a quadrantal-arc trajectory and a trajectory including a switching point. The quadrantal-arc trajectories have a single-peaked velocity profile, while the others have a coupled-profile with two single-peaked velocity profiles. It should be noticed that the coupled profile changes discontinuously around the switching time.

Through the detailed experiments with the human subjects, it was found that a human generates a single-peaked velocity profile or a double-peaked velocity profile according to the spatial trajectories. Section IV describes a method for reproducing such trajectories in manipulating a nonholonomic car.

IV. Design of a TBG-Based Controller

In this section, a feedback control law for generating a human-like trajectory for robots is designed by the TBG-based method. Fig. 7 shows a model of a unicycle-like car which a subject manipulates in the experiment. Σ_b denotes the world coordinate system (for an operational space), and Σ_c is the moving coordinate system whose origin is set at the center of two wheels of the car and the x_c axis is oriented along the direction of motion of the car. Thus, the position (x, y) and orientation angle θ of Σ_c with respect to Σ_b are chosen as the generalized coordinates of the car.

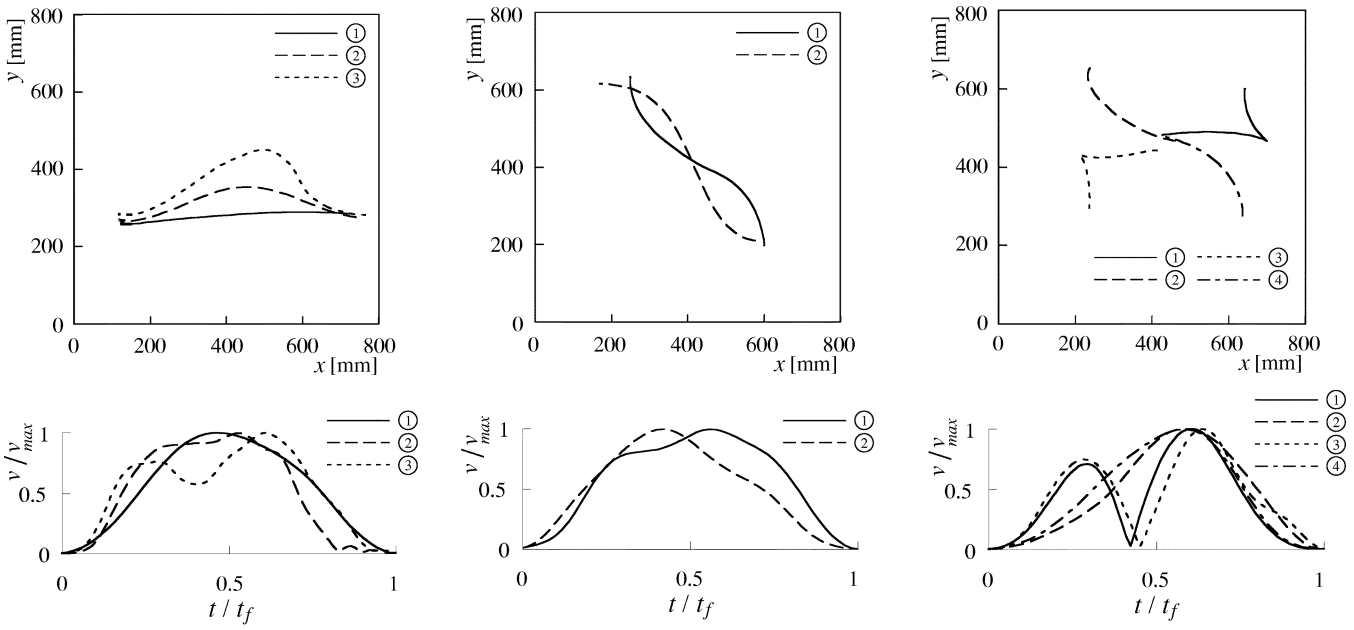

(a) Condition 1 (b) Condition 2 (c) Condition 3

Fig. 6. Generated primitive spatio-temporal trajectories under the different experimental conditions.

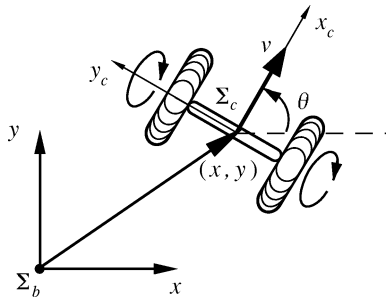

Fig. 7. Model of a vehicle with two wheels.

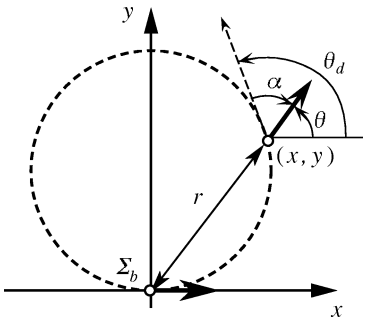

Fig. 8. Coordinate transformation.

The kinematics of the car can be described by the following equation between the time derivative of $\boldsymbol{x} = (x, y, \theta)^T$ and the linear and angular velocity of the car $\boldsymbol{u} = (v, \omega)^T$ [17]:

$$\dot{\boldsymbol{x}} = \begin{bmatrix} \cos\theta & 0 \\ \sin\theta & 0 \\ 0 & 1 \end{bmatrix} \boldsymbol{u}. \tag{11}$$

From the system (11), the following kinematic constraint can be easily derived:

$$\dot{x}\sin\theta - \dot{y}\cos\theta = 0. \tag{12}$$

Therefore, there is a nonholonomic constraint given by (12) imposed on the human hand movement while manipulating the car.

In order to design the control system, we adopt the piecewise smooth feedback control law [17] which uses a family of circles that pass through the origin and the current position of the car and contact with the x axis at the origin as shown in Fig. 8. In the figure, θ_d belonging to $[-\pi, \pi)$ represents the tangential direction of this circle at the position x.

Let α denote the angle between the tangential direction θ_d and the current angular orientation θ with the intention of designing a controller which can eliminate this kind of *orientation error* together with corresponding *position error* denoted by the distance r from the target. The following coordinate transformation from $\boldsymbol{x} = (x, y, \theta)^T$ to $\boldsymbol{z} = (r, \alpha)^T$ is then introduced [8]:

$$r(x, y) = \sqrt{x^2 + y^2} \tag{13}$$

$$\alpha(x, y, \theta) = e + 2n(e)\pi \tag{14}$$

$$e = \theta - \theta_d \tag{15}$$

$$\theta_d = 2arc\tan 2(y, x) \tag{16}$$

where $n(e)$ is the function that takes an integer in order to satisfy $\alpha \in [-\pi, \pi)$. Also, $arc\tan 2(\cdot, \cdot)$ is the scalar function defined as $arc\tan 2(a, b) = \arg(b + ja)$, where j denotes the imaginary unit and $\arg$ denotes the argument of a complex number. As a result, the current state of the car can be represented by

$$\boldsymbol{z} = \begin{bmatrix} r(x, y) \\ \alpha(x, y, \theta) \end{bmatrix} \tag{17}$$

and the target configuration is transformed from $\boldsymbol{x}_d = (0, 0, 0)^T$ to $\boldsymbol{z}_d = (0, 0)^T$.

Substituting (11) into the time derivation of (17), the relationship between $\dot{\boldsymbol{z}}$ and the system input $\boldsymbol{u}$ can be derived as

$$\dot{\boldsymbol{z}} = \boldsymbol{B}(\boldsymbol{x})\boldsymbol{u} \tag{18}$$

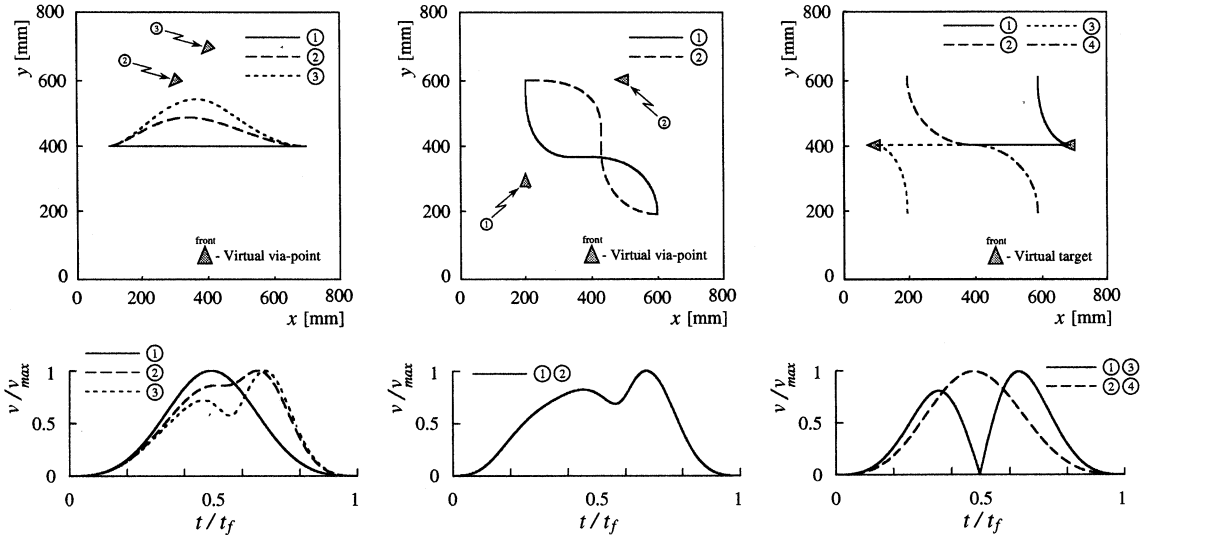

(a) Condition 1 (b) Condition 2 (c) Condition 3

Fig. 9. Generated primitive spatio-temporal trajectories by the TBG-based method under the different experimental conditions.

where

$$\boldsymbol{B}(\boldsymbol{x}) = \begin{bmatrix} b_1 & 0 \\ b_2 & 1 \end{bmatrix} \tag{19}$$

$$b_1 = -(x\cos\theta + y\sin\theta)(x^2+y^2)^{-1/2} \tag{20}$$

$$b_2 = 2(y\cos\theta - x\sin\theta)(x^2+y^2)^{-1}. \tag{21}$$

It can be seen that the number of state variables is reduced to the same number as the system input.

For the derived system (18), the following potential function V required to design the feedback controller can be defined:

$$V = \frac{1}{2}\left(k_r r^2 + k_\alpha \alpha^2\right) \tag{22}$$

where k_r and k_α are positive constants. From (10), the feedback controller $\boldsymbol{u}$ based on the potential function V in (22) can be designed as

$$\boldsymbol{u} = -\frac{1}{2}a(t)\boldsymbol{B}^{-1}(\boldsymbol{x})\left(\frac{\partial V}{\partial z}\right)^T = \begin{bmatrix} \frac{k_r p r \dot{\xi}}{2b_1\xi} \\ -b_2 v + \frac{k_\alpha p \alpha \dot{\xi}}{2\xi} \end{bmatrix} \tag{23}$$

under the assumption of $\det\boldsymbol{B}(\boldsymbol{x}) \neq 0$ except at the target position $\boldsymbol{x}_d$.

With the feedback controller $\boldsymbol{u}$, the time derivative of V yields

$$\dot{V} = \left(\frac{\partial V}{\partial z}\right)^T \boldsymbol{B}(\boldsymbol{x})\boldsymbol{u} = pV\frac{\dot{\xi}}{\xi} < 0. \tag{24}$$

As $\dot{V}$ is always negative except at the equilibrium point, the system of the car in the actual time scale is asymptotically stable by means of the designed feedback control law $\boldsymbol{u}$. Moreover, this differential equation given in (24) can be readily solved as follows [9]:

$$V = V_0\xi^p \tag{25}$$

where $V_0 = V(\boldsymbol{x}_0)$ is the initial value of V. It can be seen that the potential function V is "synchronized" with the TBG because V is proportional to the pth power of ξ. Since ξ reaches zero at t_f, so must V: in other words, the car with two wheels is bound to reach the target position $\boldsymbol{x}_d$ from the initial position $\boldsymbol{x}_0$ just at $t = t_f$ with the controller $\boldsymbol{u}$ given in (23).

V. Bio-Mimetic Trajectory Generation Based on Human Arm Movements

Human-like trajectories with a single-/double-peaked velocity profile were generated by the designed controller using the TBG. Fig. 9 shows the spatio-temporal trajectories with the conditions 1) –3) defined in Section III, in which the convergence time is set at $t_f = 2.5$ [s] under the parameters $p = 2.0$, $k_r = k_\alpha = 1.0$. The TBG parameters β_i $(i = 1, 2)$ in the controller were regulated so as to realize the suitable velocity profile according to the spatial trajectory. In the figures of the velocity profiles, the vertical axis is normalized by the maximum value $v_{\max}$ for each trial and the horizontal axis by the specified time $t_f = 2.5$ [s], respectively.

Since a spatio-temporal trajectory in both the straight and the quadrant-arc trajectories can be uniquely determined by specifying the initial and the final positions of the nonholonomic car, such human-generating trajectory can be reproduced just by determining the TBG parameters (β_i and t_f) under the given two-point condition. To the contrary, in both the out-curved and the S-shaped trajectories, the curvature of a spatial trajectory depends on voluntary motion of human subjects in maneuvering the car. Thus, various curved patters may appear only by specifying the initial and the final positions.

To express the family of such curved trajectories in the framework of the TBG model, a virtual via-point $\boldsymbol{x}_v^* = (x_v^*,\ y_v^*,\ \theta_v^*)^T$ is set on the task space as a time-varying equilibrium point of the potential field [See Fig. 9(a) and (b)], in which the virtual via-point starts moving at the time t_i^a $(i = x, y, \theta)$ and reaches the final point at the time t_i^b according to the TBG dynamic behavior as shown in Fig. 10. Here, parameters on the virtual via-point, such as $\boldsymbol{x}_v^*$ and t_i^a, were determined by manual from the experimental data in this paper, although it is desirable to design such parameters according to the desired trajectory as well as experimental conditions. Also, the virtual target posture θ_v^* is directed toward the specified final point, while control parameters of dynamic behavior of the virtual via-point were set as $\beta_1^* = \beta_2^* = 0.75$, $t_x^a = t_y^a = 0.35t_f$, $t_\theta^a = 0.1t_f$ under $|t_i^a - t_i^b| = (t_f/2)$, respectively, so that the double-peaked velocity profiles were produced.

Similarly, a switching pattern is generated by specifying a virtual target $\boldsymbol{x}_d^* = (x_d^*,\ y_d^*,\ \theta_d^*)^T$ on the target space as a switching point as shown in Fig. 9(c), in which two primitive patterns are separately generated before and after the switching time $t = (t_f/2)$ and connected at the point $\boldsymbol{x}_d^*$. The virtual target is arranged so as to represent the final

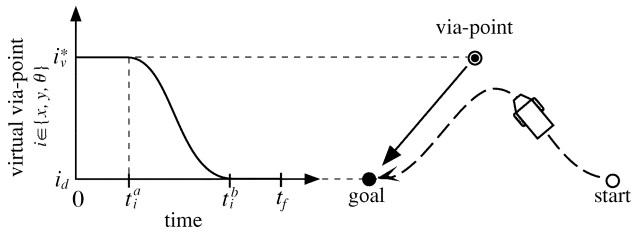

Fig. 10. Virtual via-point used in the simulations.

condition of the former pattern as well as the initial condition of the latter pattern on the basis of the observed human movements.

Fig. 9(a) shows the generated trajectories with the initial condition $\boldsymbol{x}_0 = (0.7\ [\mathrm{m}], 0.4\ [\mathrm{m}], \pi\ [\mathrm{rad}])^T$ and the target condition $\boldsymbol{x}_d = (0.1\ [\mathrm{m}], 0.4\ [\mathrm{m}], \pi\ [\mathrm{rad}],^T$ under $(\beta_1, \beta_2) = (0.75, 0.75)$. In the curved spatial trajectories ② and ③, the virtual via-point was set as $\boldsymbol{x}_v^* = (0.3\ [\mathrm{m}], 0.6\ [\mathrm{m}], (5/4)\pi\ [\mathrm{rad}])^T$, $(0.4\ [m], 0.7\ [m], (5/4)\pi\,[\mathrm{rad}])^T$, respectively. It can be observed from Fig. 9(a) that the generated curved trajectories have a double-peaked velocity profile sinking around $t = (t_f/2)$ that is similar to the observed human trajectories. Also, the velocity profile tends to be more sharply double-peaked as the curvature increases.

Fig. 9(b) shows the generated S-shaped trajectories and their velocity profiles with $\boldsymbol{x}_0 = (0.6\ [\mathrm{m}], 0.2\ [\mathrm{m}], \pi/2\ [\mathrm{rad}])^T$, $(0.6\ [\mathrm{m}], 0.2\ [\mathrm{m}], \pi\ [\mathrm{rad}])^T$ and $\boldsymbol{x}_d = (0.2\ [\mathrm{m}], 0.6\ [\mathrm{m}], \pi/2\ [\mathrm{rad}])^T$, $(0.2\ [\mathrm{m}], 0.6\ [\mathrm{m}], \pi\ [\mathrm{rad}])^T$ under $(\beta_1, \beta_2) = (0.75,\ 0.75)$. The virtual via-point of each pattern was set as $\boldsymbol{x}_v^* = (0.2\ [\mathrm{m}], 0.3\ [\mathrm{m}], \pi/2\ [\mathrm{rad}])^T$, $(0.5\ [\mathrm{m}], 0.6\ [\mathrm{m}], \pi\ [\mathrm{rad}])^T$, respectively. The simulated trajectories with a double-peaked velocity profile express the general characteristics of the observed S-shaped trajectories.

Finally, Fig. 9(c) shows the quadrantal trajectories with a single-peaked profile and the switching trajectories according to the different initial conditions $\boldsymbol{x}_0 = (0.6\ [\mathrm{m}], 0.6\ [\mathrm{m}], \pi/2\ [\mathrm{rad}])^T$, $(0.2\ [\mathrm{m}], 0.6\ [\mathrm{m}], \pi/2\ [\mathrm{rad}])^T$, $(0.2\ [\mathrm{m}], 0.2\ [\mathrm{m}], \pi/2\ [\mathrm{rad}])^T$, $(0.6\ [\mathrm{m}], 0.2\ [\mathrm{m}], \pi/2\ [\mathrm{rad}])^T$ with the target condition $\boldsymbol{x}_d = (0.4\ [\mathrm{m}], 0.4\ [\mathrm{m}], \pi\ [\mathrm{rad}])^T$. Here, in generating the switching patterns ① and ③, the virtual target was set as $\boldsymbol{x}_d^* = (0.7\ [\mathrm{m}], 0.4\ [\mathrm{m}], \pi\ [\mathrm{rad}])^T$, $(0.1\ [\mathrm{m}], 0.4\ [\mathrm{m}], \pi\ [\mathrm{rad}])^T$, respectively, while the TBG parameters β_i were changed $(\beta_1, \beta_2) = (0.75, 0.5)$ to $(\beta_1, \beta_2) = (0.5, 0.75)$ before and after the switching time $t_f/2$. The other trajectories ② and ④ were simulated without any switching points under $(\beta_1, \beta_2) = (0.75, 0.75)$. The simulated trajectories in Fig. 9(c) are resemble the observed human trajectories in Fig. 6(c) in both spatial and temporal characteristics.

Through a series of computer simulations, it can be concluded that the designed controller using TBG can generate human-like trajectories with the kinematic features of human arm movements in maneuvering a nonholonomic car by utilizing the virtual via-point/target.

VI. Conclusion

The present paper has investigated the influences of nonholonomic constraints on human arm movements in maneuvering a nonholonomic toy car from one point to another, and has tried to generate human-like trajectories for robots on the basis of human generating trajectories according to circumstances. From the experimental results, the following distinctive characteristics in the target task have been found:

- Subjects change a generating pattern depending on the initial and final conditions of the car.
- Subjects generate three types of primitive strategic patterns: a straight trajectory with a single-peaked profile, an S-shaped trajectory with a double-peaked profile, and a quadrantal-arc trajectory with a single-peaked profile.
- Subjects generate a switching trajectory by the combination of primitive patterns according to the experimental circumstances.

By applying the TBG-based method with a virtual via-point/target, the spatio-temporal trajectories of the observed human primitive strategies have been reproduced successfully.

Since the present paper has intended to reproduce primitive trajectories in human voluntary movements in the framework of a TBG model, a problem still remains: how to determine the suitable virtual via-point/target in generating human-like trajectories. In future research work, we plan to investigate the influences of via-points on human trajectory generation in the given target task through experiments with subjects, and develop an algorithm to arrange an optimal virtual via-point/target according to circumstances on the basis of experimental evidences.

References

[1] S. Hashimoto *et al.*, "Humanoid robot-development of an information assistant robot handaly," in *Proc. IEEE 8th Int. Workshop Robot Human Commun.*, 1997, pp. 106–111.

[2] K. Hirai, M. Hirose, Y. Haikawa, and T. Takenaka, "The development of honda humanoid robot," in *Proc. IEEE Int. Conf. Robot. Automat.*, 1998, pp. 1321–1326.

[3] P. Morasso, "Spatial control of arm movements," *Experimental Brain Res.*, vol. 42, pp. 223–227, 1981.

[4] T. Flash and N. Hogan, "The coordination of arm movements: An experimentally confirmed mathematical model," *Biolog. Cybern.*, vol. 57, pp. 1688–1703, 1985.

[5] Y. Uno, M. Kawato, and R. Suzuki, "Formation and control of optimal trajectory in human multi-joint arm movement," *Biolog. Cybern.*, vol. 61, pp. 89–101, 1989.

[6] D. Bullock and S. Grossberg, "VITE and FLETE: Neural modules for trajectory formation and postural control," in *Volitional Action*, W. A. Hershberger, Ed. Amsterdam, The Netherlands: North-Holland/Elsevier, 1989, pp. 253–297.

[7] P. Morasso, V. Sanguineti, and T. Tsuji, "A dynamical model for the generator of curved trajectories," in *Proc. Int. Conf. Artificial Neural Networks*, 1993, pp. 115–118.

[8] T. Tsuji, P. Morasso, and M. Kaneko, "Feedback control of nonholonomic mobile robots using time base generator," in *Proc. IEEE Int. Conf. Robot. Automat.*, 1995, pp. 1385–1390.

[9] T. Tsuji, P. Morasso, V. Sanguineti, and M. Kaneko, "Artificial force-field based methods in robotics, in self-organization, computational maps and motor control," in *Advances in Psychology*, P. Morasso and V. Sanguineti, Eds. North-Holland, The Netherlands: Elsevier, 1997, vol. 119, pp. 169–190.

[10] Y. Tanaka, T. Tsuji, M. Kaneko, and P. G. Morasso, "Trajectory generation using time scaled artificial potential field," in *Proc. IEEE/RSJ Int. Conf. Intelligent Robots Syst.*, 1998, pp. 223–228.

[11] T. Tsuji and K. Ito, "Position/force control strategies in human movements during crank rotation tasks" (in Japanese), *Japanese J. Ergonom.*, vol. 28, no. 4, pp. 209–218, 1992.

[12] K. Ohta, Z. W. Luo, and M. Ito, "Human perceptual-motor coordination in unknown dynamical environments," in *Proc. IEEE Int. Conf. Syst., Man, Cybern.*, 1997, pp. 459–462.

[13] T. Tsuji, S. Koyama, and M. Kaneko, "Adaptive ability of human operator in human-robot system" (in Japanese), in *Proc. 15th Annu. Conf. Robotic Society Japan*, vol. 2, 1997, pp. 311–312.

[14] Y. Tanaka, T. Tsuji, and M. Kaneko, "Trajectory formation of human arm with nonholonomic constraints," in *Proc. 3rd Int. Conf. Adv. Mechatron.*, vol. 2, 1998, pp. 1–6.

[15] D. A. Winter, *Biomechanics and Motor Control of Human Movement*, 2nd ed. New York: Wiley, 1990, pp. 41–43.

[16] M. Sampei and K. Furuta, "On time scaling for nonlinear systems: Application to linearization," *IEEE Trans. Automat. Contr.*, vol. AC-31, pp. 459–462, May 1986.

[17] C. C. de Witt and O. J. Sørdalen, "Exponential stabilization of mobile robots with nonholonomic constraints," *IEEE Trans. Automat. Contr.*, vol. 37, pp. 1791–1797, Nov. 1992.